Ocean Engineering 319 (2025) 120209

Contents lists available at ScienceDirect

Ocean Engineering

journal homepage: www.elsevier.com/locate/oceaneng

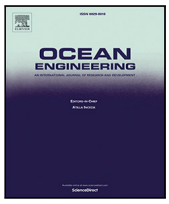

Research paper

Renewable energy systems in offshore platforms for sustainable maritime operations

Alexander Micallef [a,*], Maurice Apap [a], John Licari [a], Cyril Spiteri Staines [a], Xiao Zhaoxia [b]

[a] Department of Electrical Engineering, University of Malta, Faculty of Engineering, Msida, MSD 2080, Malta
[b] Tianjin Key Laboratory of Advanced Electrical Engineering and Energy Technology, Tiangong University, Tianjin, 300387, China

ARTICLE INFO

Keywords:
Offshore Mooring and Power Platform
Virtual power plant
Hybrid energy storage system
Offshore floating wind farm
Floating photovoltaic farm

ABSTRACT

This study presents a novel Offshore Mooring and Power Platform (OMPP) that integrates Platform-to-Ship systems to electrify anchored and bunkering ships, significantly reducing greenhouse gas emissions in maritime applications. The OMPP consists of a 200 MW floating wind farm, a 300 MW floating photovoltaic farm, and a hybrid energy storage system, forming an offshore virtual power plant to ensure reliable and continuous power supply despite the intermittency of renewable energy sources. A case study focused on the Maltese Islands demonstrates the technical feasibility of the system, utilizing a hybrid energy storage configuration comprising a 390 MWh battery energy storage system and a 1260 MWh compressed air energy storage system to eliminate energy deficit hours. The OMPP, rated at 24 MVA, successfully supplies up to four berths with 6 MVA each. While challenges remain in integrating early-stage technologies, the OMPP provides a scalable and sustainable solution for modernizing port infrastructure, meeting environmental standards, and supporting sustainable maritime operations.

1. Introduction

Growing environmental concerns and the imposition of stringent regulations are accelerating the maritime sector's shift towards sustainable practices, fostering a surge in innovative ocean engineering solutions. The European Union (EU) has enacted a comprehensive regulatory framework aimed at reducing the carbon footprint of European maritime shipping. Directive 2014/94/EU (Directive 2014/94/EU, 2014), together with the FuelEU Maritime Initiative (Directive (EU), 2016), are central to the EU's push towards greener and more sustainable maritime operations. Directive 2014/94/EU mandates that by 2025, ports within the Trans-European Transport Network (TEN-T) must integrate shore-to-ship (S2S) power supply systems. Compliance necessitates significant investment in port infrastructure and standardization to ensure efficient operation across the network.

The FuelEU Maritime Initiative, introduced by the European Commission in 2021 as a complement to Directive 2014/94/EU, mandates that ships docked in EU ports for over two hours must use shore-side power from January 2030. This initiative provides a clear regulatory framework and timeline for the maritime industry to adopt cleaner technologies and reduce its environmental footprint.

The EU efforts for significant carbon emission reductions by 2050 extend beyond these directives. The European Green Deal, including the Fit for 55 package includes proposals to extend the EU Emissions Trading System to cover maritime transport, incentivizing the reduction of emissions through a market-based mechanism. In addition, the Renewable Energy Directive II (Directive 2018/2001/EU), sets a binding renewable energy target for 2030 and encourages the use of renewable energy in the transport sector (Directive (EU) 2018/2001, 2018). The revision of the Alternative Fuels Infrastructure Directive (AFID) by EU Regulation 2023/1804 that entered in force in April 2024, aims to support the deployment of alternative fuels infrastructure, essential for the widespread adoption of electric and hydrogen-powered ships (Regulation (EU) 2023/1804, 2023).

To comply with these directives, ports must invest in the necessary infrastructure and standardize technical specifications to ensure smooth and efficient operations across the network. The development of stable, large-scale offshore structures capable of withstanding harsh marine environments is essential to this effort. Such structures must not only provide the necessary stability and load-bearing capacity but also integrate seamlessly with renewable energy systems to ensure a continuous and reliable power supply. The largest offshore structure to date, the Prelude FLNG (floating liquefied natural gas) facility which is a ship-like structure measuring 488 × 78 × 360 m, highlights the scale and complexity involved in such projects (Kaiser, 2020). In this context, Very Large Floating Structures (VLFS) have emerged as a promising technological solution.

* Corresponding author.
E-mail address: alexander.micallef@um.edu.mt (A. Micallef).

https://doi.org/10.1016/j.oceaneng.2024.120209
Received 30 August 2024; Received in revised form 9 December 2024; Accepted 22 December 2024
Available online 31 December 2024

Table 1
Types of VLFS: Advantages and Disadvantages (Lamas-Pardo et al., 2015).

VLFS	Advantages	Disadvantages
Mega-Float	Easy and cost-effective manufacturing and assembly. Modular design allows for unlimited expansion. Can support significant loads.	Only suitable for calm waters (such as inlets and bays). Low mobility, i.e. difficult to relocate once deployed. Susceptible to green water effect. Theoretical understanding still developing.
Mobile Offshore Base	High mobility; capable of moving across various locations. Versatile in both deep and shallow waters.	Restrictions on weight carrying capacity. Internal movements pose a risk of structural fatigue. Connector technology still under research. High construction and operational costs.
Pneumatically Stabilized Platform	Relatively easy and inexpensive installation. Expandable design options with minimal maintenance. Suitable for various waters, though less effective in extremely harsh environments.	Experimental design based on indirect displacement. Limited mobility once installed. Underdeveloped joining technology.
Versabuoy	Excellent reduction of wave-induced movements. Modular system allows for customization and expansion.	Complex mooring system requires intricate management. Subjected to significant vertical forces complicating deployment. Lack of mobility. Relocation is not feasible.

VLFS are designed to support substantial loads while maintaining stability in open waters, making them ideal candidates for large, sustainable platforms at sea. Although still largely theoretical, these concepts demonstrate the potential for constructing extremely large, stable structures at sea. VLFS concepts have been proposed in literature for a number of large-scale offshore applications, including floating airports, harbors, and bridges, that offer valuable insights into the engineering challenges involved (Wang and Tay, 2011). VLFS designs are classified based on their structural configurations, operational environments, and intended applications. Lamas-Pardo, Iglesias and Carral in Lamas-Pardo et al. (2015) provide an overview of existing VLFS designs, including the Mega-Float, Mobile Offshore Base, Pneumatically Stabilized Platform, and Versabuoy. Table 1 compares their advantages and disadvantages in terms of operational depth and proximity to the coast.

Recent advancements in VLFS technology, such as enhanced hydrodynamic modeling, lightweight materials, and modular designs, align with sustainable development goals and improve feasibility (Jiang et al., 2023). However, challenges such as high construction costs, maintenance complexity, and the need for comprehensive regulatory frameworks remain significant barriers. Addressing these challenges and securing public acceptance are crucial for the successful deployment of VLFS projects.

Another key technology to sustainable practices in the maritime industries is S2S, also known as cold ironing or onshore power supply (OPS). Ships, whether at berth or anchored offshore, typically rely on their main or auxiliary engines to power essential onboard systems, including lighting, cooling, heating, fuel pumps, communication equipment, and passenger/crew spaces. S2S power allows these ships to turn off these diesel engines by drawing power from the shore's electricity grid, significantly reducing emissions of pollutants and greenhouse gases such as nitrogen oxides (NO_x), sulfur oxides (SO_x), particulate matter (PM), and greenhouse gases (CO_2).

Research on electrifying berthed ships, particularly cruise vessels, is still in its infancy. Few studies have explored the potential synergies between S2S and renewable energy sources (RES) within the framework of integrated energy systems (Frković et al., 2024), highlighting a significant gap in the current body of knowledge. Bakar et al. provided a comprehensive overview of the state of the art in S2S integration at seaports in Abu Bakar et al. (2023), focusing on operational, conceptual, and standardization aspects drawn from relevant research articles, technical reports, and government studies. Their review also discusses how integrating microgrids with S2S could significantly advance the decarbonization efforts within the maritime industry. In Micallef et al. (2023), the authors summarize the state-of-the-art in port microgrid research, highlighting that there are still significant gaps that have yet to be fully explored.

A S2S system primarily consists of the shore-side power supply, connection system, and berthed ship interface, as shown in Fig. 1. The shore-side power supply serves as the critical interface between the ship and the local grid, with high-voltage shore connection (HVSC) systems offering superior power handling capabilities for large vessels than low-voltage shore connection (LVSC) systems. HVSC systems, operating at either 6.6 kV or 11 kV, have become the preferred choice due to their advanced power handling capabilities. HVSC systems are designed to handle much higher power capacities than LVSC, ranging from 6 MVA to over 20 MVA, making them suitable for larger vessels such as cruise ships and large container ships. HVSC systems can also accommodate ships with different voltage level requirements offering ports the flexibility to serve a diverse fleet. Due to the high-voltage level used in HVSC systems, the cables are heavier and bulkier than those used in LVSC. This increased weight necessitates a cable management system, such as cable reels, automated cranes, retractable arms, movable cable gantries, and guided cable trays (Khadka, 2019).

While significant progress has been made in the development of S2S power systems and the exploration of VLFS, a critical gap remains in integrating these technologies with offshore RES. Current research often addresses the individual components, such as the operational aspects of S2S or the structural challenges of VLFS, without tackling the complexities of combining these systems into a cohesive platform that provides continuous, reliable power to maritime vessels. Furthermore, many of the technologies required for this integration, such as offshore hybrid energy storage systems, are at early Technology Readiness Levels, adding another layer of complexity and uncertainty to their deployment.

Recent research also highlights the potential of hybrid renewable energy systems combining, for example, wind and solar energy with advanced storage technologies to address energy intermittency and achieve decarbonization goals in maritime and offshore applications. For example, Ikuerowo et al. (2024) proposed green hydrogen production systems utilizing water electrolyzers powered by renewable sources as an alternative for long-term energy storage and integration with offshore platforms. Similarly, Effatpanah et al. (2023) employed solid oxide fuel cell and gas turbine-based zero-carbon cogeneration systems to simultaneously meet energy demands and environmental targets. These integrated systems demonstrate the versatility of hybrid configurations in tackling complex energy challenges, offering valuable insights into scalability and environmental performance.

VLFS platforms, with their stability and load-bearing capacity in open waters, are particularly well-suited to host S2S systems, resulting in Platform-to-Ship (P2S) capabilities that offer a sustainable energy solution for vessels at sea, including hybrid and electric ships. This study addresses the existing research gap by proposing and evaluating

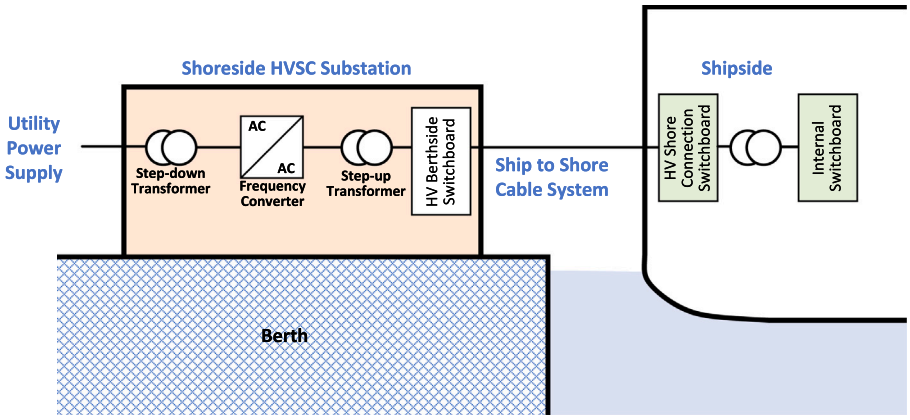

Fig. 1. Main components of a S2S system. *Source:* Adapted from Sciberras et al. (2015).

an innovative Offshore Mooring and Power Platform (OMPP) within the Maltese national waters. The OMPP integrates a 200 MW offshore wind farm, a 300 MW photovoltaic (PV) farm, and a hybrid energy storage system (HESS) to support sustainable maritime operations. Although the offshore HESS considers technologies that are at early TRLs, these technologies are critical for managing energy storage and distribution in offshore settings. The combination of offshore RES and HESS form a renewable-based virtual power plant (VPP) that ensures continuous power supply despite the intermittent nature of the RES. The detailed concept of the OMPP is presented in the following sections.

The OMPP represents a significant advancement in maritime energy solutions by merging multiple RES with a platform designed to moor and power multiple ships. Unlike traditional approaches that rely on onshore power grids or single-source renewable systems, the OMPP combines offshore wind and solar power with hybrid energy storage, ensuring a reliable energy supply even under variable conditions. This integrated approach not only supports decarbonization of maritime operations but also demonstrates the feasibility of using VLFS technology to create sustainable energy hubs at sea. By reducing reliance on fossil fuels and improving air quality, the OMPP aligns with EU sustainability objectives and showcases advanced VLFS technology in compliance with stringent EU directives. The platform is designed to supply energy to anchored or bunkering vessels offshore, addressing the growing need for cleaner maritime fuel options. This capability supports green maritime transitions in Maltese ports and serves as a model for other coastal nations aiming to modernize their maritime infrastructure while meeting environmental goals.

The rest of this paper is organized as follows: Section 2 introduces the concept of a renewable-based OMPP integrating a VPP with Platform-to-Ship (P2S) capabilities, tailored to Malta's energy needs. Section 3 addresses the design and integration of a 200 MW offshore wind farm, focusing on local wind profiles, turbine selection, energy yield analysis, and the challenges of wind energy intermittency. Section 4 examines the integration of a 300 MW PV farm to complement the wind farm, including PV module selection, environmental impact considerations, and performance analysis. Section 5 details the sizing of a HESS that combines BESS and CAES, outlining a two-stage optimization methodology, performance evaluation, and cost-effectiveness, demonstrating that a 390 MWh BESS and 1260 MWh CAES effectively eliminate energy deficits. Section 6 concludes the paper with a summary of the key findings.

2. Renewable-powered OMPP system concept

The overall system concept of the OMPP integrating an offshore renewable-powered VPP and P2S capabilities is illustrated in Fig. 2. The offshore VPP is designed to supply renewable energy to both the Maltese shore power system and the OMPP, enhancing the island's energy security and reducing its reliance on imported fossil fuels. The capacities of the wind and PV farm were sized based on a minimum load demand of 300 MW observed during Spring 2022 (source: Enemalta plc). Point-to-point high voltage direct current (HVDC) transmission is employed for the interconnection of the offshore VPP with the onshore power system to optimize power transmission efficiency.

The OMPP connects to the offshore VPP via a medium voltage direct current (MVDC) link, approximately 20 km in length. The platform, with estimated dimensions of 1200 × 300 m, is designed to accommodate up to four ships each up to 200 m long. It features a 24 MVA P2S facility with four berths each providing up to 6 MVA. The platform dimensions are based on a 20 m buffer zone on each side of the ships, allowing for four ships to dock comfortably with a safety margin for operational flexibility. The P2S facility enables ships to connect to the platform electrical grid while docked, reducing the reliance on onboard diesel generators and significantly cutting emissions. The VPP must provide consistent power to meet the base load demand of 24 MVA set by the OMPP, even during periods of low RES availability. The HESS plays a critical role, storing excess energy during high production and releasing it when the wind power and PV generation are low, ensuring uninterrupted power to the OMPP.

In literature, energy storage systems (ESS) can be classified into six main categories based on their mode of energy storage: mechanical, electrical, chemical, electrochemical, thermal, and thermochemical (Kandari et al., 2023; Rabanal et al., 2024). While pumped hydro storage is a popular and mature technology for managing wind power, it is not suitable for Malta due to the island's flat topography and water scarcity. Battery energy storage systems (BESS) offer a more viable solution for Malta's energy needs, particularly for managing the intermittent nature of RES. However, BESS deployment onshore faces significant challenges, including limited land availability and high population density (Micallef et al., 2022).

Offshore ESS solutions, such as subsea compressed air energy storage (SCAES) (Pimm and Garvey, 2016) and offshore pumped hydro storage, present promising solutions for Malta but they are still in the early development stages. Offshore BESS is another option, though it involves technical complexities. This study focuses on a hybrid storage configuration combining floating platform-integrated BESS and SCAES. BESS is effective for short-term storage, addressing fluctuations from seconds to hours, while SCAES manages medium to long-term storage by compressing air in subsea reservoirs and generating electricity when needed. Integrating SCAES with offshore wind and PV infrastructure presents challenges due to high construction and maintenance costs in deep-sea environments but represents a promising approach for Malta's energy needs.

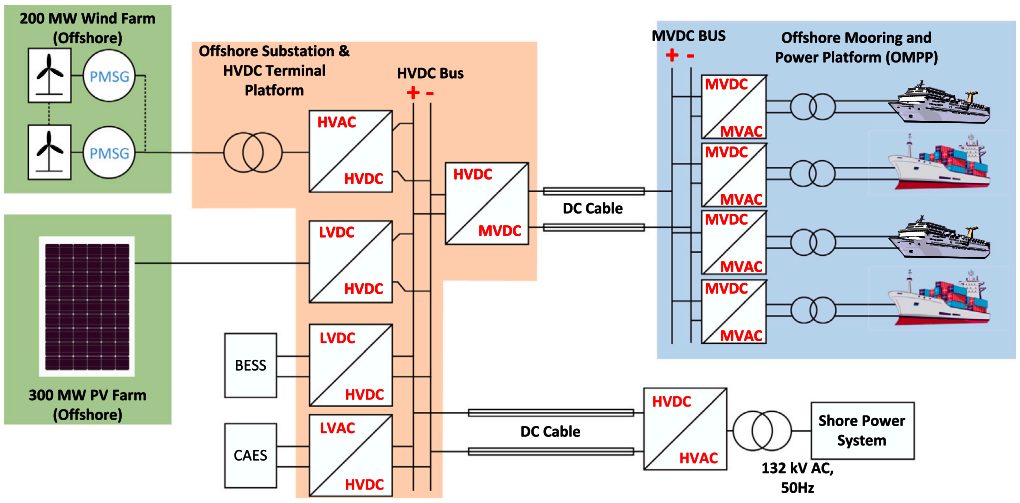

Fig. 2. Block diagram of the renewable-powered offshore mooring and power platform concept.

The Technology Readiness Levels (TRL) and Commercial Readiness Levels (CRL) of the considered offshore components were determined prior to the sizing and evaluation of the integration challenges. These levels indicate the maturity and commercial viability of the considered technologies and can be summarized as follows:

- Fixed-bottom offshore wind: This technology is considered fully mature with a TRL of 9, reflecting its widespread deployment in offshore wind farms. The CRL is at 9, as these systems are commercially available and have been successfully deployed at scale in various regions.
- Floating offshore wind: Floating wind turbine technology is rapidly advancing, with a TRL of 8–9 depending on foundation types. However, the CRL is estimated at 3–4, as commercial deployment is still in the early stages, particularly for large-scale offshore applications.
- Inland floating solar: Floating solar technology for inland applications has reached TRL 9, demonstrating readiness for deployment. However, the CRL remains low at around 3, since commercial deployment is still limited.
- Offshore floating solar: Offshore floating solar technology is at relatively mature at TRL of 6–8, indicating readiness for large-scale deployment. However, the CRL is low at 2, due to the scarcity of commercial installations in offshore environments.
- Offshore floating battery storage: Battery storage technologies such as lithium-ion are mature with a TRL of 8–9, but the integration of these systems into floating offshore platforms is still under development, reducing the overall TRL to 4–6. The CRL is 1–2, since commercialization for offshore applications is limited.
- Offshore subsea compressed air energy storage (CAES): The core technology for CAES is relatively mature, with a TRL of 4–6. However, integrating CAES with subsea infrastructure and optimizing it for long-term offshore storage is still under development, leading to a CRL of 1–2.

Addressing these TRL and CRL challenges will be crucial for the future success and scalability of the proposed OMPP system.

3. Site selection methodology

The site selection process for the offshore floating RES, HESS and the OMPP was driven by technical criteria to ensure optimal performance and integration with existing maritime infrastructure. The following summary outlines the key technical criteria used in selecting the sites for the RES, ESS and the OMPP.

3.1. Floating RES and ESS site selection

Six potential areas for offshore renewable energy development within the Maltese exclusive economic zone (EEZ) were identified in the National Policy for the Deployment of Offshore Renewable Energy (Energy and Water Agency, 2023). These areas were selected based on environmental impact assessments, which included wind profile analysis, comprehensive seabed and geotechnical studies, and considerations such as seabed composition, structural stability, and overall environmental impact (PRJ-ENV767 AIS Environment, 2024). Water depth is a significant factor influencing the feasibility of installing wind turbines. Malta's offshore waters vary in depth, with potential development areas having deep bathymetry (>50 m). To date, fixed offshore turbines have been installed up to depths of 60 m, with the deepest fixed installation in Scotland's Angus region reaching 58 m in 2023. However, the zones identified for potential offshore wind farm development in Malta are located in deeper waters (>73 m), which are beyond the present reach of fixed offshore turbines. As a result, floating offshore turbines are the only viable option for these areas. In addition to wind resources, the Maltese EEZ also offers significant solar energy potential. The region benefits from high levels of solar irradiance, making it an ideal candidate for the deployment of floating offshore PV systems.

From these areas, Area 3 shown in Fig. 3, was selected as a primary candidate for the 200 MW offshore wind farm and the 300 MW floating PV farm. This area covers a 1157 km^2 zone around Hurd's Bank and was deemed to have the greatest potential due to its relatively shallow offshore characteristics compared to the other sites. The water depth ranges between 73 m and 170 m, making it suitable for floating wind turbine technologies. Additionally, the distance of Area 3 from shore (specifically to Delimara power station) also offers a balance between minimizing visual impact and ensuring efficient grid connection. The 132 kV high voltage alternating current (HVAC) distribution network in this area can accommodate the expected energy output from the offshore VPP.

3.2. OMPP site selection

Malta's strategic position in the Mediterranean, particularly as a key maritime hub, makes it an ideal location for the deployment of the OMPP. The Vessel Traffic Services (VTS) manages six designated bunkering areas off Malta's coast, allocating ships to respective areas to ensure smooth traffic flow and minimize congestion (Transport Malta, 2024). Among these, Bunkering Area 3, shown in Fig. 3, was selected as the site for the OMPP, driven by several critical factors.

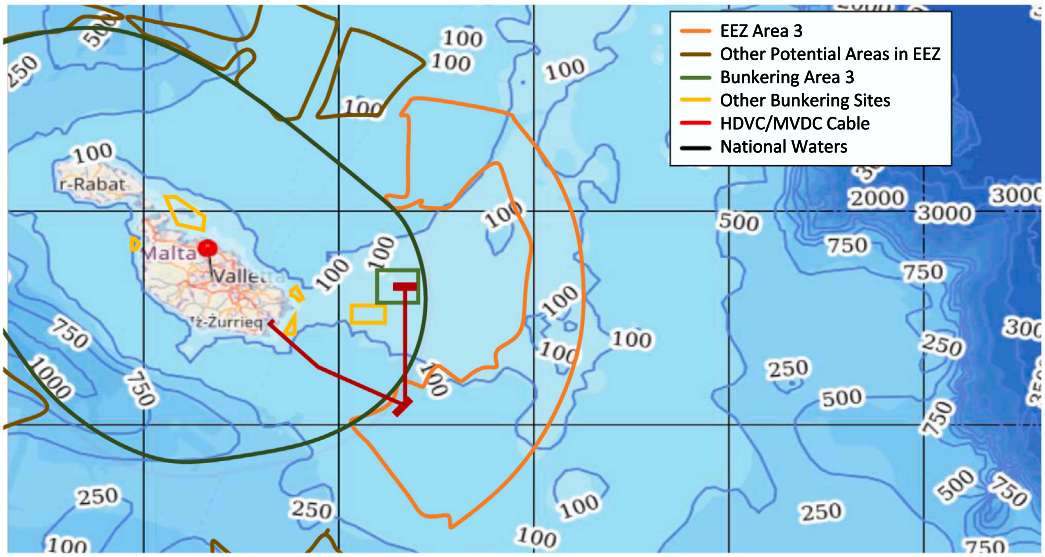

Fig. 3. Considered sites of the OMPP and VPP floating substation with estimated cable routes. [Derived product from the GEBCO 2021 Grid, made with OpenStreetMap by OpenDEM. The depth data are from OpenSeaMap Water Depths Project. https://map.openseamap.org/].

Bunkering Area 3 is strategically located along one of the busiest maritime corridors in the Mediterranean, making it ideal for offering renewable energy-powered bunkering services, aligning with the global shift towards greener maritime practices. The existing bunkering infrastructure, including operational facilities and more than 17 bunker barges (Transport Malta, 2021), provides a robust foundation for integrating the OMPP. This infrastructure allows for a smoother transition to renewable energy bunkering, minimizing the need for extensive new construction.

The site's selection also considered environmental impact assessments, ensuring that the OMPP deployment would not significantly disrupt local ecosystems. The integration of the OMPP is designed to enhance the sustainability of existing operations, reducing the carbon footprint associated with traditional bunkering activities. This strategic choice ensures that the OMPP contributes positively to both the local environment and broader maritime sustainability goals.

By selecting Bunkering Area 3 for the OMPP, the project capitalizes on existing maritime infrastructure while advancing Malta's leadership in sustainable maritime practices, ensuring the site supports both operational efficiency and environmental stewardship. This aligns with Malta's commitment to sustainability and innovation in its maritime sector. The OMPP represents a significant step forward in modernizing maritime infrastructure, supporting the transition to cleaner energy sources and more efficient technologies, consistent with international environmental standards.

4. Wind farm design and integration

The previous section identified locations for the offshore VPP and OMPP. This section focuses on the design and integration of a 200 MW wind farm at these selected sites to ensure efficient and sustainable energy production. Detailed estimations of the hourly power profile and total energy yield are provided, which are essential for evaluating the wind farm's performance and viability.

4.1. Local wind profile analysis

Understanding the local wind profile is crucial for designing the 200 MW wind farm. This study analyzed wind speed, direction, and variability using data from two primary sources: the Malta Airport MetOffice (Malta Airport MetOffice, 2024) and ERA reanalysis datasets (Copernicus Climate Change Service, 2020). The ERA reanalysis dataset provides offshore forecasts of wind speed data at a height of 100 m, which aligns with the rotor hub height for offshore wind turbine analysis. In contrast, the Malta Airport Met Office dataset includes maximum and minimum wind speeds at 10 m above sea level, measured at the Valletta weather station.

Weibull distributions were fitted to model wind speed data, deriving probability density functions (PDFs) and cumulative distribution functions (CDFs) as shown in Fig. 4. PDFs illustrate the frequency of different wind speeds, highlighting the most common values and their distributions. CDFs show the probability of wind speeds being below specific thresholds, shedding light on the likelihood of different wind speeds, with a CDF value of 0.5 representing the median wind speed.

From Fig. 4a, the median wind speed for the ERA reanalysis dataset is 5.76 m/s. In contrast, the median wind speed for the MetOffice maximum wind speed dataset is higher at 6.74 m/s, indicating a frequent occurrence of more intense wind events. For the mean wind speed obtained from the MetOffice dataset, the CDF reaches 0.5 at 4.3 m/s.

The PDF plots in Fig. 4b offer further detail on wind speed distributions. For the maximum wind speed profiles of 2022 and 2023, the shape parameter (α) is approx. 1.8, which denotes a moderately peaked distribution. The scale parameters (β) for these years are around 8.0 m/s and 8.2 m/s, respectively which are higher than the reanalysis and mean wind speed datasets. In comparison, the reanalysis data for the same years have an α of 1.7 and a β of 7.3 m/s, reflecting a similar peak but with less extreme values. For mean wind speeds, α is around 1.7 with a β of 5.9 m/s, suggesting a distribution with a wider spread and less pronounced peak. When observing the PDF peaks, the maximum wind speeds have a peak at 5.4 m/s, the reanalysis wind speeds peak at 4.15 m/s, while the mean wind speeds show a peak around 3 m/s.

Finally, Fig. 5 presents a polar histogram that illustrates the wind direction data for the maximum wind speeds recorded in Malta for the years 2022 and 2023. As anticipated, the histogram confirms that the most prevalent wind direction is from the northwest, known locally as the Majjistral. Given the similarity in wind speed profiles between the two datasets, the authors opted to use the Met Office data for wind direction and speed. While it is common to extrapolate wind speeds from 10 m to 100 m for similar studies, this adjustment was not applied in this case due to the similarities observed between the two profiles (from the ERA dataset and the Malta Airport Met Office

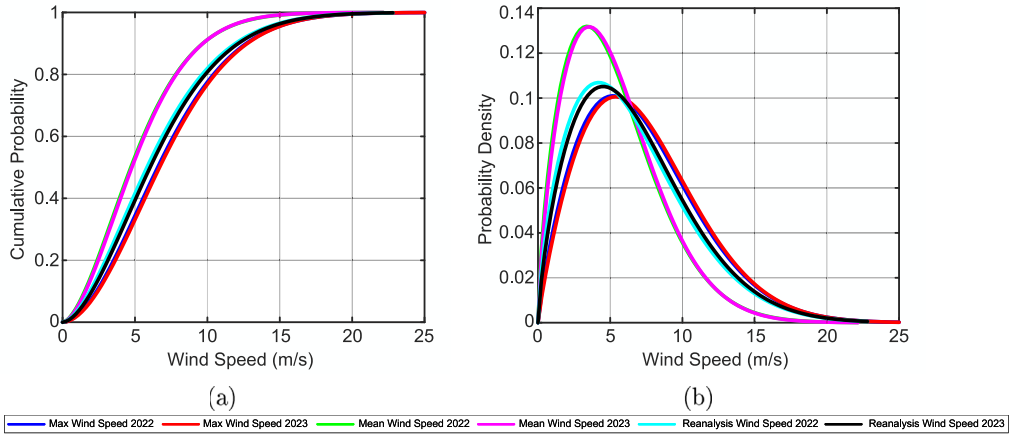

Fig. 4. Analysis of the Malta Airport MetOffice and ERA reanalysis datasets. (a) Cumulative distribution functions. (b) Probability density functions.

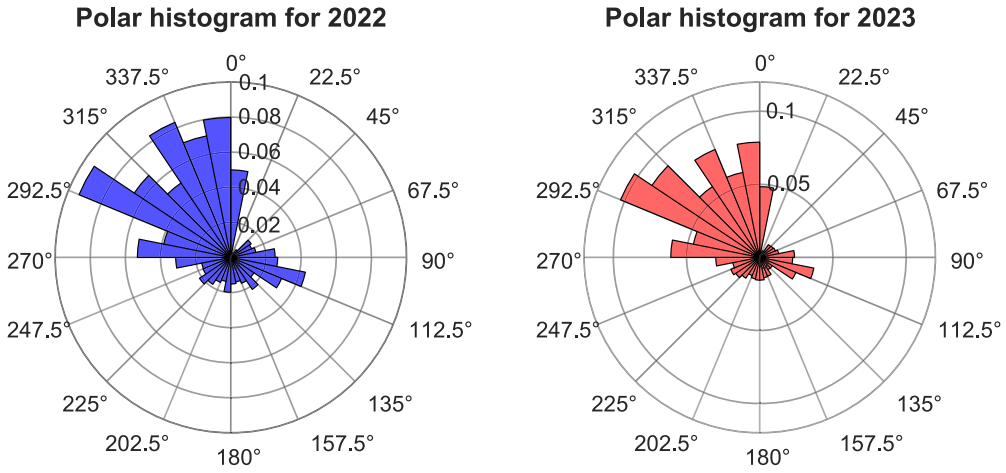

Fig. 5. Polar histogram of the wind direction data for the maximum wind speeds recorded in Malta for the years 2022 and 2023.

dataset). Therefore, it was assumed that the wind profiles from the Met Office data exhibits similar trends at 100 m.

4.2. Wind energy systems

The insights from the local wind profile analysis were used to select appropriate turbine models to estimate the potential energy production based on local conditions. The analysis focused on determining the energy yield per area required (GWh/km^2) for each turbine, using their power curves and hourly wind data.

Table 2 compares parameters of four commercially available offshore turbines. The choice of turbine models was influenced by the wind profiles observed at the site, with consideration given to the typical rotor hub heights found in offshore wind farms. A standard rotor hub height of 100 m was assumed in this study, which is commonly used for modern offshore wind turbines. The median for local wind speeds range from 4.3 m/s to 6.74 m/s, as detailed in the wind profile analysis. While the World Bank (and some other organizations) recommend a minimum annual mean wind speed of 7 m/s for wind farms to be considered profitable, the wind speeds observed at the site, although slightly below this threshold, are still within the feasibility range for offshore wind farms, especially when hybrid energy storage systems are employed to manage intermittency. Thus, these wind speeds remain relevant to the scope of this study, supporting the feasibility of wind energy projects in Malta. Thus, turbines with a broad operational range and robust performance in varying wind conditions were prioritized. Turbines with lower cut-in speeds and higher rated capacities were preferred to maximize energy capture, particularly given the moderate wind speeds at the site. The selected turbines are commercially available and have a proven track record in offshore applications. All four turbines are well-suited to the site's wind conditions, making them suitable choices for efficient and sustainable energy production.

4.2.1. Power curve analysis

To estimate the energy yield for each of the four turbines, The power curves were analyzed using the parameters outlined in Table 2. The power curve of each wind turbine can be divided into distinct regions based on the wind speed (Deshmukh and Deshmukh, 2008). These regions are defined as:

- Region 1: Wind speeds below the cut-in speed ($0\,\text{m/s} \leq V < V_{\text{cut-in}}$). In this region, the turbine power output is zero as the wind speed is insufficient to overcome the mechanical resistance and initiate operation.
- Region 2: Wind speeds between the cut-in speed and the rated speed ($V_{\text{cut-in}} \leq V < V_{\text{rated}}$). The power output increases from zero to the rated power as wind speed rises, with the output determined by the wind speed relative to the cut-in and rated speeds.
- Region 3: Wind speeds between the rated speed and the cut-out speed ($V_{\text{rated}} \leq V < V_{\text{cut-out}}$). The turbine operates at its maximum rated power during this interval.
- Region 4: Wind speeds above the cut-out speed ($V \geq V_{\text{cut-out}}$). In this region, the turbine shuts down to prevent damage from excessive wind speeds, resulting in no power generation.

Table 2
Relevant parameters of four commercially available offshore turbines.
Source: Manufacturer websites.

Manufacturer	Turbine model	Power rating (MW)	Rotor diameter (m)	Cut-in wind speed (m/s)	Rated wind speed (m/s)	Cut-out wind speed (m/s)
Siemens Gamesa Renewable Energy	SG 8.0–167 DD	8	167	3	12	25
GE Renewable Energy	Alstom Haliade 150-6 MW	6	150	3	12	25
MHI Vestas Offshore Wind	Offshore V164-9.5 MW	9.5	164	3.5	14	25
Goldwind	GW 184/6450	6.45	184	3	10	21

The turbine power output $P(V)$ curve can be modeled by Deshmukh and Deshmukh (2008) and Abeg et al. (2024):

$$P(V) = \begin{cases} 0, & \text{for } 0 \le V < V_{\text{cut-in}} \\ P_{\text{rated}} \left(\frac{V^3 - V_{\text{cut-in}}^3}{V_{\text{rated}}^3 - V_{\text{cut-in}}^3} \right), & \text{for } V_{\text{cut-in}} \le V < V_{\text{rated}} \\ P_{\text{rated}}, & \text{for } V_{\text{rated}} \le V < V_{\text{cut-out}} \\ 0, & \text{for } V \ge V_{\text{cut-out}} \end{cases} \quad (1)$$

This analysis enables the comparison of the performance of different turbines by evaluating their power output across various wind speeds. Understanding how each turbine performs in these regions helps in selecting the most suitable turbine models for the wind conditions at the site, ensuring optimal energy capture and system efficiency.

4.2.2. Performance of the turbines under real-world conditions

The theoretical power curves and energy yield estimates provide an initial understanding of turbine performance. However, real-world conditions introduce additional factors such as wind shear, turbulence, temperature variations, and mechanical wear that can affect turbine efficiency. In the case of floating wind turbines, movement of the platform due to waves can cause misalignment between the turbine and the optimal wind direction. While modern turbines are designed to automatically orient themselves toward the wind, the movement of the floating platform introduces some variability in the alignment. This misalignment, though generally small, can still impact the overall efficiency of the turbine, particularly in rougher sea conditions. As certain wind directions may be more favorable depending on local topography and wind patterns, this effect could slightly influence energy capture. Although the automatic orientation mechanism reduces the direct impact of wind direction on turbine efficiency, the platform's movement adds another layer of complexity that needs to be considered.

Yaw angle variations were integrated into the power output calculations to incorporate real-world complexities. Yaw misalignment, which occurs when the turbine is not perfectly aligned with the wind direction, can lead to significant efficiency losses. This study adopted a simplified method to estimate the impact of yaw misalignment on performance, avoiding the complexity of Computational Fluid Dynamics (CFD) simulations.

The effective wind speed at any given hour h, was adjusted based on the yaw misalignment angle. This angle, denoted as $\theta_{\text{mis,h}}$, represents the absolute difference between the wind direction and the turbine orientation. This was determined by:

$$\theta_{\text{mis,h}} = \min\left(\left| \theta_{\text{wind,h}} - \theta_{\text{turbine}} \right|, 360° - \left| \theta_{\text{wind,h}} - \theta_{\text{turbine}} \right| \right) \quad (2)$$

where $\theta_{\text{wind,h}}$ is the direction from which the wind is blowing (degrees) at hour h, and θ_{turbine} is the direction the turbine is facing (degrees). To quantify the impact of yaw misalignment, the yaw angle factor at hour h, was defined as:

$$\text{YAF}_{\text{h}} = \cos\left(\theta_{\text{mis,h}}\right) \quad (3)$$

where the magnitude of YAF_{h} ranges from 0 to 1. A value of 1 indicates perfect alignment with no efficiency loss, while values approaching 0 reflect increasing misalignment.

Table 3
Total energy yield per area (in GWh/km^2) per turbine for the max effective hourly wind speed. The turbine orientation was assumed fixed at 305 degrees.

Turbine model	Turbine area (km^2)	Max. direction		Min. direction	
		2022 ($\frac{\text{GWh}}{\text{km}^2}$)	2023 ($\frac{\text{GWh}}{\text{km}^2}$)	2022 ($\frac{\text{GWh}}{\text{km}^2}$)	2023 ($\frac{\text{GWh}}{\text{km}^2}$)
SG 8.0–167 DD	1.9522	5.19	6.04	4.82	5.29
Alstom Haliade 150-6 MW	1.575	4.82	5.61	4.48	4.92
Offshore V164-9.5 MW	1.8827	4.51	4.70	4.26	4.64
GW 184/6450	2.3699	4.68	5.38	4.23	4.66

The effective wind speed was then calculated by adjusting the original wind speeds with the YAF_{h}. For example, the effective wind speeds at hour h for the measured maximum wind speeds were determined by $V_{\text{eff,max,h}} = V_{\text{max,h}} \times \text{YAF}_{\text{h}}$. Finally, the power output of each turbine model at hour h, $P_{\text{h}}(V)$, was determined by applying these adjusted effective wind speeds to the power curve Eq. (1).

4.2.3. Simulations and analysis

Simulations were then performed in MATLAB to evaluate the energy yield of each wind turbine model and to assess how different turbine orientations affect efficiency. Turbine orientations were varied from 270 to 360 degrees in 5-degree increments. The simulations used site-specific wind data and adjusted for yaw misalignment to apply each turbine's power curve and estimate energy output. The goal was to identify the optimal turbine orientations and models for maximizing energy generation.

Figs. 6 and 7 show the total energy yield against the turbine orientation for the maximum effective wind speeds at the maximum and minimum wind directions. These results show that turbines with larger rotor diameters, such as the Goldwind GW 184/6450, show higher energy yields due to increased swept area capturing more wind energy. In addition, an orientation of 305 degrees consistently resulted in higher energy yields across all turbines, suggesting it is the optimal orientation for the wind farm.

4.2.4. Turbine total energy yield per area

Table 3 presents the total energy yield per area for each turbine model, expressed in GWh/km^2, based on maximum and minimum effective hourly wind speeds for 2022 and 2023. The turbine orientation was fixed at 305 degrees.

The SG 8.0–167 DD consistently provides the highest energy yield per area, with 6.04 GWh/km^2 in 2023 for the maximum wind direction and 5.29 GWh/km^2 for the minimum wind direction. As expected, all turbines perform better under the maximum wind direction, which emphasizes the importance of wind directionality in optimizing energy output. While the SG 8.0–167 DD is the most efficient in terms of energy yield per area, final turbine selection should also consider site-specific factors such as installation costs and environmental impacts.

4.3. Wind farm power output

To estimate the hourly power output of the wind farm, the maximum wind speed data from 2022 and 2023 was used alongside the

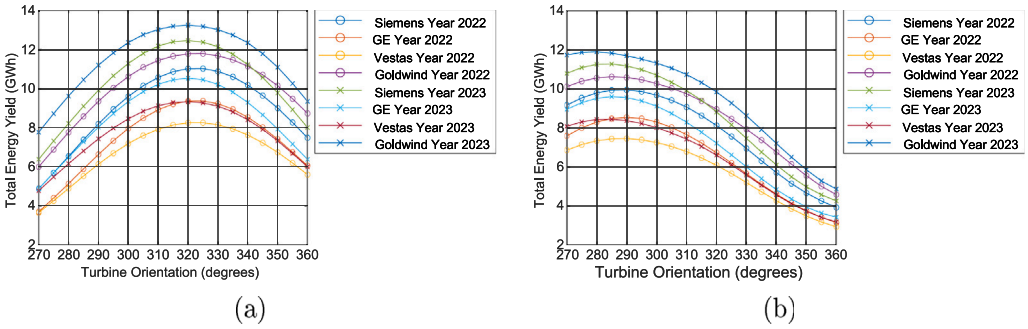

Fig. 6. Energy yield for the four turbines for 2022 and 2023 with the maximum wind direction dataset adjusted for yaw misalignment. (a) Max effective wind speed. (b) Mean effective wind speed.

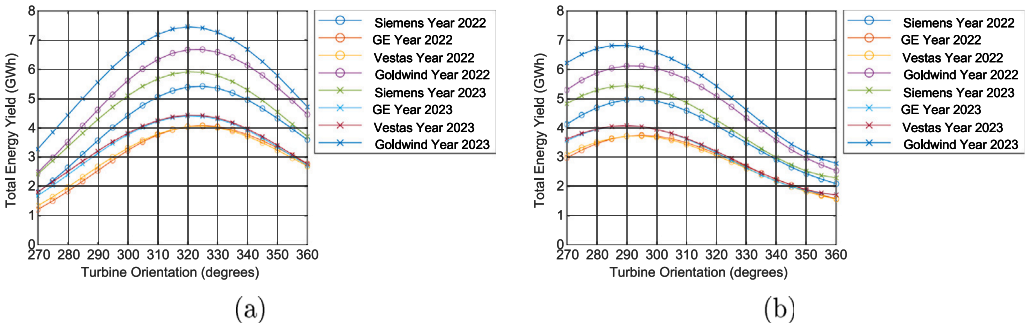

Fig. 7. Energy yield for the four turbines for 2022 and 2023 with the minimum wind direction dataset adjusted for yaw misalignment. (a) Max effective wind speed. (b) Mean effective wind speed.

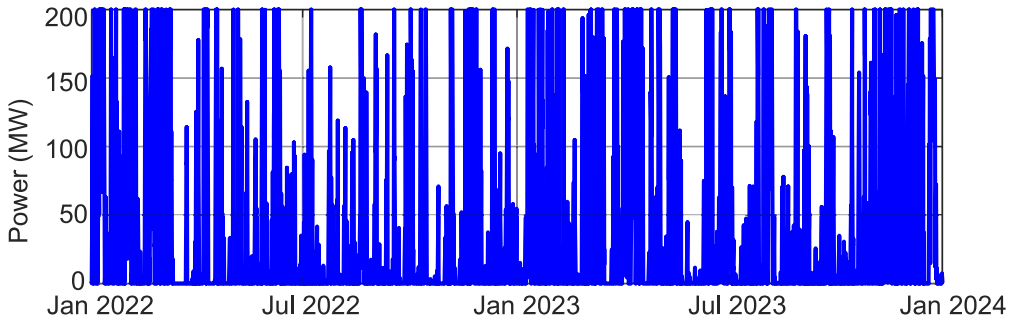

Fig. 8. Hourly power output profile of the 200 MW wind farm using maximum wind speed data.

power curve of the SG 8.0–167 DD turbine. The hourly power output for a single turbine under peak wind conditions was determined and scaled to reflect the total number of turbines in the 200 MW wind farm, estimated to be 25. Turbine spacing was approximated to minimize wake interference, simplifying the analysis and focusing on the potential energy yield of each turbine model without the need for complex wake modeling. Turbines were assumed to be spaced in multiples of rotor diameters (D), where it was assumed that the spacing was of 10D in the prevailing wind direction and 7D perpendicular to the prevailing wind direction.

The scaled hourly power output is illustrated in Fig. 8 shows the wind farm's production potential. The capacity factor (CF) of the wind farm was determined by:

$$\mathrm{CF} = \left(\frac{\text{Total Energy Produced (MWh)}}{\text{Installed Capacity (MW)} \times \text{Hours Per Period}} \right) \times 100 \quad (4)$$

where Total Energy Produced (MWh) is the sum of the hourly power output over the period, Installed Capacity (MW) is the nominal capacity of the wind farm, and Hours Per Period is the total number of hours in the two-year period. For the floating wind farm, the capacity factor over the two-year period was calculated to be 31.29% and 28.16% for the maximum and minimum wind profile, respectively.

The wind farm's potential as a standalone VPP is significantly limited by its inherent intermittency, which can result in extended periods without power generation. The most severe instance occurred in March 2022, where the wind farm fails to produce any power output for 11 consecutive days. Another similar event happened in April 2022, lasting 6 days. Additionally, there were several instances throughout the year where the wind farm did not generate sufficient power to supply the OMPP, with a total of 12 790 h. These interruptions highlight the local variability and intermittency challenges associated with wind energy, which impact the reliability of the supplied power.

5. PV farm sizing and integration

Given the intermittency of the wind farm's power generation, integrating a PV farm is crucial to achieve a stable and reliable supply. Malta's abundant solar resource, characterized by consistent sunlight throughout the year, effectively complements the variability of wind energy. By integrating a 300 MW PV farm, the energy production gaps caused by low wind speeds can be mitigated, resulting in a more balanced and reliable renewable-based VPP system. This integration

significantly enhances the overall capacity factor of the combined energy system.

5.1. PV module selection

The choice of PV module type determines the system's efficiency, durability, and suitability for the offshore environment. For this analysis, SunPower Maxeon 3 SPR-MAX3-430 [Monocrystalline Maxeon Gen 3] were used, having a high efficiency of 22.7% at STC and reliability, due to compliance with IEC 61701 for salt spray testing (maximum severity) (SunPower, 2022). The panel dimensions are 1812 × 1046 mm with a nominal power output of 430 W at STC and a power temperature coefficient of −0.27% °C. SunPower Maxeon 3 modules were also recently considered in floating PV farm study for the neighboring island of Lampedusa (Ghigo et al., 2022).

The PV farm was considered to utilize a horizontal panel orientation. The optimal tilt angle of 30 degrees, commonly used for maximizing solar exposure in Malta was sacrificed in favor of mitigating wind stress and shading issues. However, this horizontal orientation may result in a reduction in solar energy capture, particularly during periods of low sun angles, such as in winter.

5.2. Baseline power output of the PV farm

Measured solar irradiance data from the Malta Airport MetOffice for 2022 and 2023 (Malta Airport MetOffice, 2024) was used to model the hourly power output of these horizontally oriented PV panels. The dataset includes measured hourly maximum and minimum solar irradiance values and ambient temperatures, together with forecast daily sea temperatures. This irradiance data inherently accounts for the effects of cloud cover and other atmospheric conditions on solar irradiance.

The baseline power output of the PV farm at hour h enables the estimation of the PV farm's power output based on real-world irradiance conditions, providing a basis for evaluating its performance over time. It was defined using the standard relation:

$$P_{PV,h} = P_{STC}\frac{G_{mean,h}}{G_{STC}} \tag{5}$$

where $P_{PV,h}$ is the output power of the PV farm at hour h, P_{STC} is the output power of the PV farm under standard test conditions and $G_{mean,h}$ is the mean solar irradiance at hour h.

5.3. Temperature and wind corrections

Environmental factors impact the performance and efficiency of PV modules, especially in an offshore environment. To improve the power output estimation for the floating PV farm, factors including the wind speed, ambient temperature, sea temperature, and the effect of sea water cooling were also included.

5.3.1. Ambient temperature correction

Ambient temperature significantly impacts PV module efficiency, as the modules' performance is sensitive to temperature changes. Elevated ambient temperatures lead to higher module temperatures, which in turn reduce efficiency due to increased temperature-induced losses. To account for these effects, the hourly power output of the PV modules was adjusted by Skoplaki and Palyvos (2009):

$$P_{PV,corr,h} = P_{PV,h}\left(1 + \gamma_{P,temp}\cdot(T_{module,h} - T_{STC})\right) \tag{6}$$

where $\gamma_{P,temp}$ is the temperature coefficient of the PV modules (−0.27/% °C), and T_{STC} is the reference temperature of 25 °C.

5.3.2. Sea water cooling

The floating PV modules in an offshore setting benefit from the cooling effect of the surrounding sea water, which can significantly reduce module temperatures and associated efficiency losses. To integrate sea water cooling into the temperature model, the hourly temperature of the PV modules ($T_{module,h}$) was adjusted by a simplified linear model relying on general cooling principles. This model was defined as:

$$T_{module,h} = T_{ambient,h} - \left(T_{ambient,h} - T_{sea,h}\right)\cdot\gamma_{sea} \tag{7}$$

where $T_{module,h}$ is the effective temperature of the PV module, $T_{ambient,h}$ is the ambient air temperature, $T_{sea,h}$ is the sea water temperature, and γ_{sea} is the correction factor representing the efficiency of the cooling system. A constant correction factor of 0.6 was used that indicates that sea water cooling is reasonably effective. This correction is applied only when the sea temperature is lower than the ambient temperature.

5.3.3. Wind speed effects

Wind speed affects the cooling of PV panels with higher wind speeds generally enhancing the cooling effect, further reducing the module temperature. The relationship between wind speed and module temperature was estimated by the well known Faiman's module temperature model (Faiman, 2008):

$$T_{module,h} = T_{ambient,h} + \frac{G_{mean,h}}{U_0 + U_1 \times V_{wind,h}} \tag{8}$$

where $T_{module,h}$ is the module temperature at hour h, $T_{ambient,h}$ is the ambient temperature at hour h, $G_{mean,h}$ is the mean solar irradiance at hour h, U_0 and U_1 are heat transfer coefficients, and $V_{wind,h}$ is the wind speed at hour h.

5.4. Adjusted PV farm hourly output

The adjusted hourly power output of the PV farm, considering all environmental factors, was determined by:

$$P_{PV,corr,h} = N\cdot P_{PV,h}\left(1 + \gamma_{P,temp}\cdot(T_{module,h} - T_{STC})\right) \tag{9}$$

where $T_{module,h} = T_{ambient,h} - \left(T_{ambient,h} - T_{sea,h}\right)\cdot\gamma_{sea,h} - \gamma_{wind}\cdot V_{wind,h}$ is the hourly temperature of the PV modules considering both the sea water cooling and wind speed effects and N is the number of modules in the 300 MW PV farm. The scaled hourly power output in Fig. 9 provides a comprehensive overview of the energy production potential.

The capacity factor of the floating PV farm over the two year period was of 21.8%. The capacity factor is influenced by the local climate and environmental conditions. Hence, the integration of wind cooling and sea water cooling into the temperature correction model allows for a more realistic estimate of the PV farm's performance, ultimately resulting in a more reliable capacity factor calculation.

The addition of the PV farm has significantly improved the supply reliability, reducing instances of extended periods without power generation. However, the offshore VPP still failed to generate sufficient power to supply the OMPP for a total of 8057 h (reduction of 37%). These interruptions highlight the critical importance of introducing ESSs within the VPP.

6. Hybrid energy storage sizing

The integration of ESSs allows excess energy generated during periods of high RES availability to be stored and then discharged during periods of low generation, such as calm nights or overcast days. This ensures a continuous and stable power supply to the OMPP, effectively bridging the gap between energy production and demand, and significantly enhancing the overall reliability and resilience of the VPP.

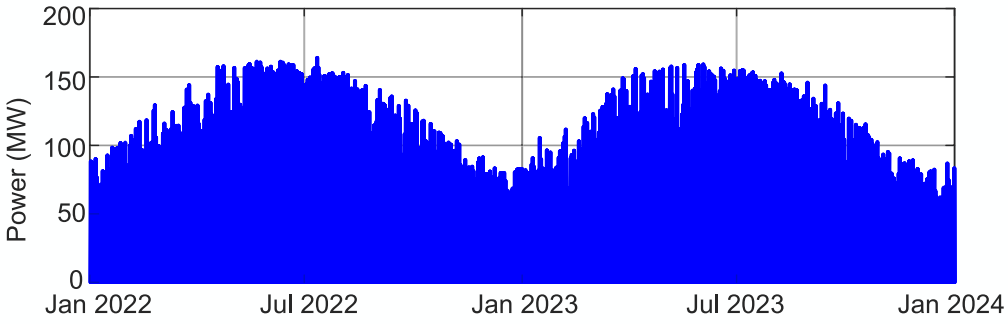

Fig. 9. Hourly power output profile of the 300 MW PV farm.

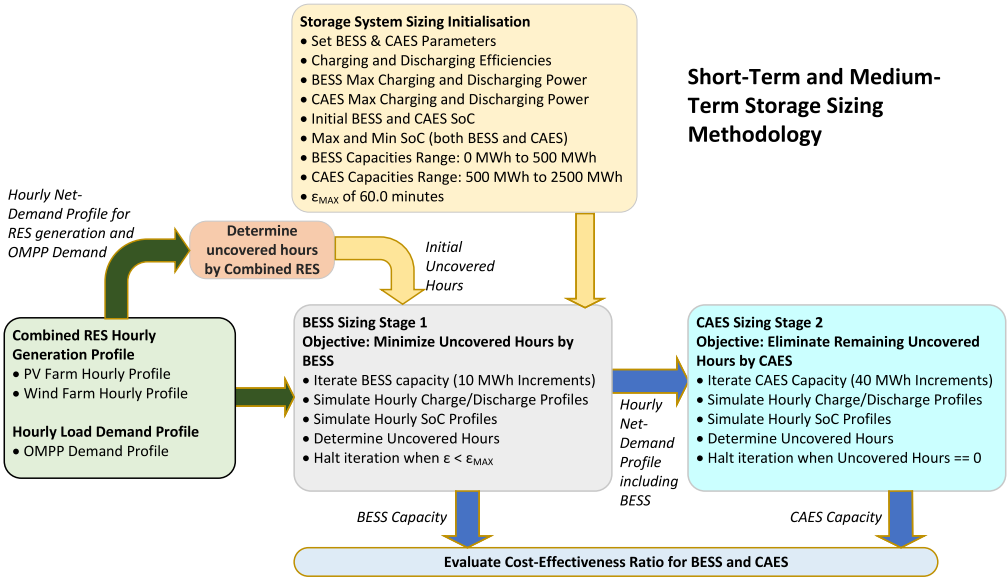

Fig. 10. Sizing strategy for hybrid energy storage systems to minimize energy deficits.

6.1. BESS and CAES capacity sizing methodology

The flowchart in Fig. 10 illustrates the methodology used to optimize the capacities of both the BESS and CAES, aiming to minimize energy deficits while ensuring cost-effectiveness. In the first stage, the BESS was optimized to reduce the number of hours when power generation fell below the OMPP's base load. BESS capacities were evaluated in 10 MWh increments, ranging from 0 MWh to 500 MWh. The optimization process simulated the charging and discharging behavior for each BESS capacity, storing excess energy during periods of surplus generation and discharging during deficits. Hourly state of charge (SoC) profiles were tracked to ensure adherence to the operational limits. A threshold criterion, ϵ, defined as a predetermined level of minimal improvement, was used to determine when further increases in BESS capacity would yield negligible reductions in energy deficit hours, thereby efficiently identifying the optimal capacity.

In the second stage, the CAES system was sized to address longer-duration power deficits that the BESS could not handle. CAES capacities ranging from 500 MWh to 2500 MWh, in increments of 40 MWh, were simulated alongside the optimized BESS to assess their combined effectiveness in reducing energy deficit hours. The CAES system's SoC was also monitored to ensure it operated within specified limits. The optimal CAES capacity was selected based on its ability to minimize energy deficit hours after the BESS deployment.

The power balance equation at the VPP terminal station at hour 'h', was defined as:

$$P_{VPP,h} = P_{WF,h} + P_{PV,h} + P_{charge,bess,h} - P_{discharge,bess,h} + P_{charge,caes,h} - P_{discharge,caes,h} \quad (10)$$

where $P_{VPP,h}$ is the power at the VPP terminal station; $P_{WF,h}$ is the electricity generated by the offshore wind farm; $P_{PV,h}$ is the electricity generated by the floating PV farm; $P_{charge,bess,h}$ and $P_{discharge,bess,h}$ are the power charged and discharged by the BESS, respectively; $P_{charge,caes,h}$ and $P_{discharge,caes,h}$ are the power charged and discharged by the CAES, respectively. Power losses on the MVDC transmission link was assumed to be at 1% per 100 km, while the efficiency for the MVDC to MVAC conversion at the OMPP was assumed constant at 97%.

Constraints critical for the operation of both BESS and CAES systems are summarized in Table 4, including round-trip efficiencies, SoC ranges, power limits, and energy conservation equations.

6.2. HESS simulation results

Fig. 11 presents the results of the two-stage methodology for sizing the hybrid storage. In Stage 1 (Fig. 11a), the BESS was optimized using a 60-min threshold criterion to determine when further capacity increases provided minimal reductions in energy deficit hours. This led to an optimal BESS capacity of 390 MWh, reducing deficit hours to 2023. Although increasing the capacity to 500 MWh would further

Table 4
Table of BESS and CAES Constraints.

Constraint	BESS	CAES
Round-trip energy efficiency	$\eta_{bess,round\text{-}trip} = 85\%$	$\eta_{caes,round\text{-}trip} = 64\%$
Charging efficiency	$\eta_{charge,bess} = 92.2\%$	$\eta_{charge,caes} = 80\%$
Discharging efficiency	$\eta_{discharge,bess} = 92.2\%$	$\eta_{discharge,caes} = 80\%$
Hourly SoC Range	$20\% \leq SoC_{actual,bess,h} \leq 80\%$	$0\% \leq SoC_{actual,caes,h} \leq 100\%$
Max discharge power	$P_{discharge,bess,max} = 25$ MW	$P_{discharge,caes,max} = 25$ MW
Max charge power	$P_{charge,bess,max} = 25$ MW	$P_{charge,caes,max} = 25$ MW
Energy conservation	$E_{actual,bess,h} = E_{actual,bess,h\text{-}1} + E_{charge,bess,h} - E_{discharge,bess,h}$	$E_{actual,caes,h} = E_{actual,caes,h\text{-}1} + E_{charge,caes,h} - E_{discharge,caes,h}$
Initial SoC	20% at t = 0 s	50% at t = 0 s

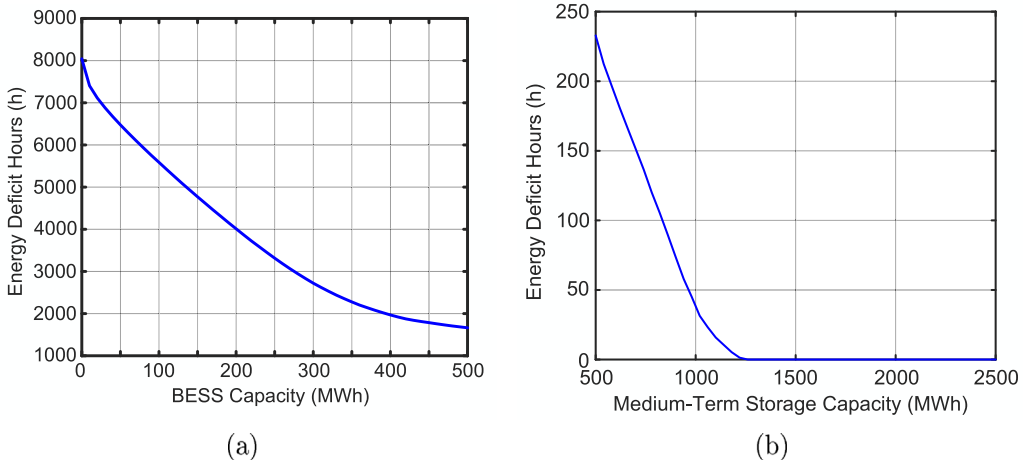

Fig. 11. Energy deficit hours during which OMPP cannot be serviced by VPP (a) Only BESS capacity. (b) CAES capacity combined with a 390 MWh BESS.

reduce deficit hours to 1664, the additional capital costs outweighed the marginal benefits.

The cost-effectiveness of BESS capacity increments was analyzed across the entire range. For each BESS capacity increment, the Cost Effectiveness Ratio (CER) was calculated to assess how efficiently the capacity increase reduced energy deficit hours. The CER at each capacity step was defined as the percentage increase in capital cost relative to the reduction in energy deficit hours achieved by the additional capacity. Capital costs were calculated based on a fixed cost per MWh of storage, and the difference between two consecutive steps corresponded to the cost of the 10 MWh increment. The reduction in energy deficit hours was the difference between the deficit hours at the two consecutive steps. Since the capacity increment is fixed at 10 MWh, the CER formula simplifies to the ratio of this 10 MWh increment to the product of the previous capacity and the reduction in deficit hours (then multiplied by 100% for a percentage indicator), allowing for a clear comparison of cost-effectiveness across capacity steps. The CER for the 390 MWh BESS was 0.032% per deficit hour, while at 500 MWh, it increased to 0.092% per deficit hour. The lower CER for the 390 MWh capacity indicates it is more cost-effective, achieving a significant reduction in deficit hours for a smaller relative increase in cost. The rising CER at higher capacities suggests diminishing returns in cost-effectiveness.

In Stage 2 (Fig. 11b), the SCAES system was sized with the BESS capacity fixed at 390 MWh. The analysis identified an optimal CAES capacity of 1260 MWh, which effectively eliminated all energy deficit hours. The cost-effectiveness of CAES capacity increments was evaluated across the entire range in steps of 40 MWh, with the CER calculated at each step to measure the efficiency of the capacity increase in reducing energy deficit hours. Capital costs were calculated using a fixed cost per MWh of storage, with the difference between consecutive steps corresponding to the cost of the 40 MWh increment. The CER for the 1260 MWh CAES was 0.085% per deficit hour. Beyond this capacity, further increases yielded no additional benefits, resulting in CER values that became infinite due to a division by zero as there can be no further reductions in the energy deficit hours.

Fig. 12 illustrates the hourly operation of the HESS over a two-year period, detailing the hourly SoC variations for both the BESS and the CAES, as well as the hourly VPP generation. From this figure, it is evident that the BESS handled short-term fluctuations in renewable energy output and sustained demand from the OMPP. The daily SoC variations remained well within the predefined operational limits of the system, demonstrating the BESS's effectiveness in managing short-term energy balancing. This is particularly evident during periods of high variability in renewable energy generation, where the BESS stabilized the system by discharging energy to meet immediate demand and recharged during surplus generation.

The CAES system, designed for medium-term storage, showed fewer but more significant discharge cycles compared to the BESS. Over the two-year period, the CAES was only required to engage in six high discharge cycles, which align with periods of prolonged low renewable energy generation and sustained demand from the OMPP. This highlights its role as a reserve system, providing stability during energy deficits that extend beyond the capacity of the BESS.

The complementary roles of the BESS and CAES in the HESS framework are also evident. The BESS primarily addresses day-to-day fluctuations in renewable energy availability, while the CAES steps in to manage longer-duration imbalances, effectively bridging the gap during extended periods of low renewable energy generation. Together, these systems ensure the reliability and resilience of the energy supply. The VPP's output power, as shown in Fig. 12, demonstrates the combined impact of the wind and PV farms alongside the HESS. The inclusion of energy storage reduces the variability of the power output compared to a system relying solely on wind and PV farms. This results in a more stable and consistent energy supply, which is critical for reliably meeting the OMPP's electricity demands.

Fig. 13 provides a closer examination of specific periods in the HESS operational timeline, further highlighting the interactions between the BESS and CAES under varying conditions. Fig. 13a focuses on a long

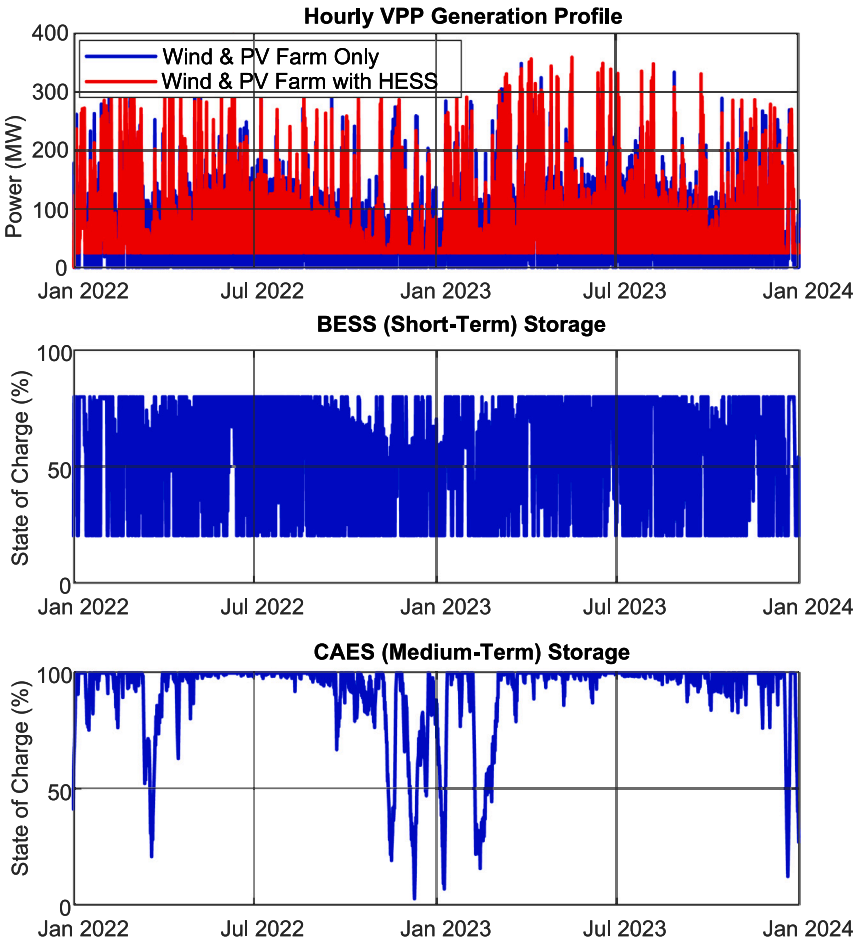

Fig. 12. Output power of the VPP considering the 1260 MWh CAES combined with a BESS of 390 MWh, including the respective hourly SoC variations of both energy storage systems.

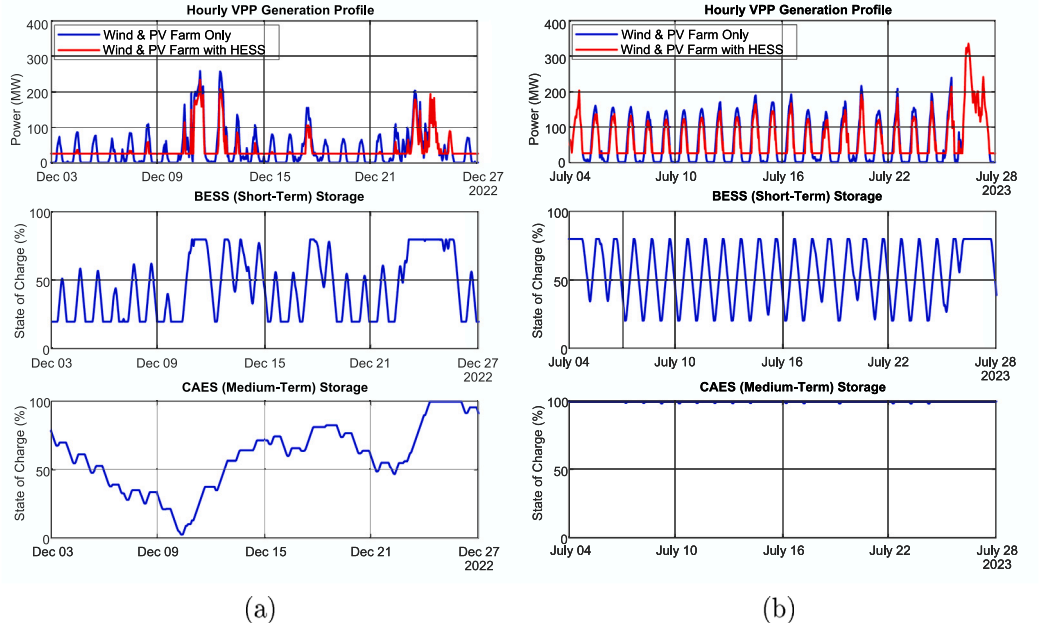

Fig. 13. Detailed views of the hybrid energy storage system's operation during critical periods: (a) A low RES generation period in December 2022, showing significant CAES discharge to address medium-term energy deficits alongside BESS activity. (b) A renewable surplus period in January 2023, where the BESS efficiently absorbs excess energy while the CAES remains inactive.

period with low wind speeds in December 2022. For instance, between the 3rd and 9th December 2022, the VPP output power curve was dominated by the PV farm, with peak generation reaching less than 100 MW due to low solar availability. The BESS actively stabilizes the VPP output by discharging energy to meet immediate demand and recharging during surplus generation. However, the limited available generation prevents the BESS from reaching the maximum threshold of 80% SoC. The CAES complements the BESS during sustained energy deficits. It discharges energy to meet electricity demand when the BESS SoC reaches its minimum threshold of 20% and recharges only when the BESS reaches the maximum SoC of 80% (during surplus generation).

Fig. 13b highlights a period of renewable energy surplus in July 2023. The VPP output is predominately from the PV farm only, with wind generation contributing significantly during the last two days of the period. During the surplus periods, the BESS cycles daily by discharging energy to meet immediate OMPP demand and recharging during surplus renewable generation. The CAES remains inactive with its SoC maintained at 100%, as no medium-term energy balancing is required during this period.

The trends observed in Figs. 12 and 13 highlight the effectiveness of the HESS in reducing the variability of the VPP output. By stabilizing fluctuations in renewable energy generation, the HESS ensures a consistent and reliable power supply for the OMPP's operational demands. This reduction in variability reflects the robustness of the HESS, with the BESS managing short-term fluctuations and the CAES providing medium-term support during energy deficits. The modularity of these systems enables scalability, allowing the HESS to be adapted for larger systems or increased energy demands. For instance, the layered storage approach can easily accommodate additional storage capacity, making the system suitable for future expansions or broader applications in renewable energy integration. By minimizing periods of energy deficit and optimizing energy storage and release, the HESS demonstrates its capability to maintain system reliability under a wide range of conditions. These characteristics not only ensure the resilience of the OMPP but also position the HESS as a scalable solution for diverse energy systems requiring integration of renewable sources.

7. Conclusion

This study presents the development and analysis of an Offshore Mooring and Power Platform integrated with Platform-to-Ship systems, aimed at reducing greenhouse gas emissions in maritime applications through the electrification of anchored and bunkering ships. The comprehensive case study focused on the Maltese islands demonstrates that the Offshore Mooring and Power Platform, powered by a 200 MW wind farm, a 300 MW PV farm, and supported by a hybrid energy storage system, can effectively supply up to four berths with high voltage shore connections, contributing to a significant reduction in emissions and improved energy reliability.

A detailed sizing analysis of the offshore battery energy storage system and subsea compressed air energy storage was conducted to optimize the energy storage capacity and ensure seamless power supply. The analysis revealed that a BESS capacity of 390 MWh is necessary to meet the short-term demands, while the CAES system, with a capacity of 1260 MWh, provides additional energy security during prolonged periods of low renewable generation. This configuration ensures that the Offshore Mooring and Power Platform can maintain a reliable power supply to the berths under varying operational conditions. The simulation-based assessments confirmed the technical viability of the Offshore Mooring and Power Platform, though the study also identified several economic and technical challenges that still need to be addressed.

Future work should focus on optimizing the cost structure, possibly through modular designs or alternative financing models, to enhance the economic attractiveness of such systems. Additionally, comparative studies with other renewable energy integration approaches in maritime or offshore settings could provide valuable insights into scalability and cost-effectiveness. These analyses would help contextualize the Offshore Mooring and Power Platform's advantages and limitations, offering further guidance on its implementation in diverse port environments. Continued research into more efficient and cost-effective energy storage technologies will also be essential to improving the performance and scalability of the Offshore Mooring and Power Platform.

The broader implications of the OMPP extend beyond its technical viability, offering a pathway for global maritime decarbonization. By aligning with European Union sustainability goals, such as those outlined in the European Green Deal, the Offshore Mooring and Power Platform could support the transition to sustainable maritime transport, accelerate the adoption of zero-emission port operations, and contribute to compliance with stricter environmental regulations. Furthermore, the implementation of Offshore Mooring and Power Platform systems at ports worldwide could have far-reaching impacts on policy development, incentivizing renewable energy adoption and shaping regulations that promote cleaner, more efficient port infrastructures.

In conclusion, while the Offshore Mooring and Power Platform offers significant environmental benefits by reducing emissions and supporting renewable energy integration, it is important to also consider potential ecological concerns associated with large floating structures and renewable energy installations in maritime environments. These concerns include impacts on marine life, potential seabed disturbances, and the physical footprint of such systems. Further research into mitigating these ecological impacts will be essential to ensure that the transition to renewable energy in maritime environments is both technically and ecologically sustainable. The successful implementation of the Offshore Mooring and Power Platform could play a pivotal role in modernizing port infrastructure, aligning with international maritime decarbonization goals, and fostering a greener future for the shipping industry.

CRediT authorship contribution statement

Alexander Micallef: Writing – original draft, Visualization, Project administration, Methodology, Investigation, Funding acquisition, Formal analysis, Data curation, Conceptualization. **Maurice Apap:** Writing – review & editing, Validation, Project administration, Methodology, Conceptualization. **John Licari:** Writing – original draft, Validation, Funding acquisition, Conceptualization. **Cyril Spiteri Staines:** Writing – review & editing, Validation, Methodology. **Zhaoxia Xiao:** Writing – review & editing, Project administration, Funding acquisition, Conceptualization.

Declaration of competing interest

The authors declare the following financial interests/personal relationships which may be considered as potential competing interests: Alexander Micallef reports financial support was provided by Malta Council for Science and Technology. Zhaoxia Xiao reports financial support was provided by Ministry of Science and Technology of the People's Republic of China. If there are other authors, they declare that they have no known competing financial interests or personal relationships that could have appeared to influence the work reported in this paper.

Acknowledgments

This work received funding from the Malta Council for Science and Technology (MCST) and the Ministry for Science and Technology of the People's Republic of China (MOST), through the SINO-MALTA Fund 2023 Call (Science and Technology Cooperation). Grant agreements: SINOMALTA-2023-01 and 2023YFE0198100.

References

Abeg, A.I., Islam, Md. R., Hossain, Md. A., Ishraque, Md. F., Islam, Md. R., Hossain, M.J., 2024. Capacity and operation optimization of hybrid microgrid for economic zone using a novel meta-heuristic algorithm. J. Energy Storage 94, 112314. http://dx.doi.org/10.1016/j.est.2024.112314.

Abu Bakar, N.N., Bazmohammadi, N., Vasquez, J.C., Guerrero, J.M., 2023. Electrification of onshore power systems in maritime transportation towards decarbonization of ports: A review of the cold ironing technology. Renew. Sustain. Energy Rev. 178, 113243. http://dx.doi.org/10.1016/j.rser.2023.113243.

Copernicus Climate Change Service, 2020. Climate and energy indicators for europe from 1979 to present derived from reanalysis. In: Copernicus Climate Change Service (C3S) Climate Data Store. CDS, http://dx.doi.org/10.24381/cds.4bd77450, (Accessed 06 August 2024).

Deshmukh, M.K., Deshmukh, S.S., 2008. Modeling of hybrid renewable energy systems. Renew. Sustain. Energy Rev. 12 (1), 235–249. http://dx.doi.org/10.1016/j.rser.2006.07.011.

Directive 2014/94/EU, Directive 2014/94/EU of the European Parliament and of the Council of 2014 on the deployment of alternative fuels infrastructure. http://data.europa.eu/eli/dir/2014/94/oj.

Directive (EU), Directive (EU) 2016/802 of the European Parliament and of the Council of 11 2016 relating to a reduction in the sulphur content of certain liquid fuels. http://data.europa.eu/eli/dir/2016/802/oj.

Directive (EU) 2018/2001, Directive (EU) 2018/2001 Directive (EU) 2018/ of the European Parliament and of the Council of 11 2018 on the promotion of the use of energy from renewable sources (recast). http://data.europa.eu/eli/dir/2018/2001/oj.

Effatpanah, S.K., Reza Rahbari, H., Ahmadi, M.H., Farzaneh, A., 2023. Green hydrogen production and utilization in a novel SOFC/GT-based zero-carbon cogeneration system: A thermodynamic evaluation. Renew. Energy 219, 119493. http://dx.doi.org/10.1016/j.renene.2023.119493, Part 2.

Energy and Water Agency, 2023. National Policy for the Deployment of Offshore Renewable Energy. https://energywateragency.gov.mt/wpcontent/uploads/2023/08/MEE-National-Policy-23_-DIGITAL-.pdf (Accessed 31 July 2024).

Faiman, D., 2008. Assessing the outdoor operating temperature of photovoltaic modules. Prog. Photovolt.: Res. Appl. 16, 307–315. http://dx.doi.org/10.1002/pip.813.

Frković, L., Ćosić, B., Falkoni, A., Pukšec, T., Vladimir, N., 2024. Shore-to-ship: Enabling the electrification sustainability of maritime transport with the nexus between berthed cruise ships and renewables in the isolated energy systems. Ocean Eng. 302, 117537. http://dx.doi.org/10.1016/j.oceaneng.2024.117537.

Ghigo, A., Faraggiana, E., Sirigu, M., Mattiazzo, G., Bracco, G., 2022. Design and analysis of a floating photovoltaic system for offshore installation: The case study of lampedusa. Energies 15, 8804. http://dx.doi.org/10.3390/en15238804.

Ikuerowo, T., Om Bade, S., Akinmoladun, A., Aisosa Oni, B., 2024. The integration of wind and solar power to water electrolyzer for green hydrogen production. Int. J. Hydrog. Energy 76, 75–96. http://dx.doi.org/10.1016/j.ijhydene.2024.02.139.

Jiang, C., Xu, P., Bai, X., Zhao, Z., el Moctar, O., Zhang, G., 2023. A review of advances in modeling hydrodynamics and hydroelasticity for very large floating structures. Ocean Eng. 285, 115319. http://dx.doi.org/10.1016/j.oceaneng.2023.115319, Part 1.

Kaiser, M.J. (Ed.), 2020. Appendix A - offshore development records CIRCA 2020. In: The Offshore Pipeline Construction Industry. Gulf Professional Publishing, pp. 359–385. http://dx.doi.org/10.1016/B978-0-12-820288-3.00022-6.

Kandari, R., Neeraj, Micallef, A., 2023. Review on recent strategies for integrating energy storage systems in microgrids. Energies 16, 317. http://dx.doi.org/10.3390/en16010317.

Khadka, J., 2019. Alternative cable technology for shore connection charging. Department of electrical technology;. https://site.uit.no/ladeteknologi/2019/09/16/alternative-cable-technology-for-shore-connection-charging/ (Accessed 31 July 2024).

Lamas-Pardo, M., Iglesias, G., Carral, L., 2015. A review of very large floating structures (VLFS) for coastal and offshore uses. Ocean Eng. 109, 677–690. http://dx.doi.org/10.1016/j.oceaneng.2015.09.012.

Malta Airport MetOffice, 2024. Comprehensive Maltese Weather Dataset for 2022 and 2023. Meteorological Office MIA plc., 2024.

Micallef, A., Guerrero, J.M., Vasquez, J.C., 2023. New horizons for microgrids: From rural electrification to space applications. Energies 16, 1966. http://dx.doi.org/10.3390/en16041966.

Micallef, A., Spiteri Staines, C., Cassar, A., 2022. Utility-scale storage integration in the maltese medium-voltage distribution network. Energies 15, 2724. http://dx.doi.org/10.3390/en15082724.

Pimm, A., Garvey, S.D., 2016. Chapter 7 - underwater compressed air energy storage. In: Letcher, Trevor M. (Ed.), Storing Energy. Elsevier, pp. 135–154. http://dx.doi.org/10.1016/B978-0-12-803440-8.00007-5.

PRJ-ENV767 AIS Environment, 2024. Environmental Report for Malta's National Policy for the Development of Offshore Renewable Energy, As Per SEA Requirements of S.L.549.61. Prepared by AIS Environment for the Energy and Water Agency (EWA), https://energywateragency.gov.mt/wp-content/uploads/2024/03/20240314_SEA-Env-report_v4.pdf (Accessed 31 July 2024).

Rabanal, A., Macmillan Smith, A., Ahaotu, C.C., Tedeschi, E., 2024. Energy storage systems for services provision in offshore wind farms. Renew. Sustain. Energy Rev. 200, 114573. http://dx.doi.org/10.1016/j.rser.2024.114573.

Regulation (EU) 2023/1804, Regulation (EU) 2023/1804 of the European Parliament and of the Council of 13 2023 on the deployment of alternative fuels infrastructure, and repealing Directive 2014/94/EU. http://data.europa.eu/eli/reg/2023/1804/oj.

Sciberras, E.A., Zahawi, B., Atkinson, D.J., 2015. Electrical characteristics of cold ironing energy supply for berthed ships. Transp. Res. D 39, 31–43. http://dx.doi.org/10.1016/j.trd.2015.05.007.

Skoplaki, E., Palyvos, J.A., 2009. On the temperature dependence of photovoltaic module electrical performance: A review of efficiency/power correlations. Sol. Energy 83 (5), 614–624. http://dx.doi.org/10.1016/j.solener.2008.10.008.

SunPower, 2022. SPR-MAX3-430 datasheet. Online Available: https://sunpower.maxeon.com/int/sites/default/files/2022-05/sp_max3_112c_415-430_res_dc_ds_en_a4_544455.pdf (Accessed 14 August 2024).

Transport Malta, 2021. Maritime services in malta. Ports & yachting directorate, authority for transport in malta, malta transport centre. https://www.transport.gov.mt/maritime/local-waters/maritime-services-in-malta-120 (Accessed 31 July 2024).

Transport Malta, 2024. Vessel traffic services. https://www.transport.gov.mt/maritime/local-waters/vessel-traffic-services-vts/vessel-traffic-services-6434 (Accessed 31 July 2024).

Wang, C.M., Tay, Z.Y., 2011. Very large floating structures: Applications, research and development. Procedia Eng. 14, 62–72. http://dx.doi.org/10.1016/j.proeng.2011.07.007.